Journal of Materials Chemistry A

Accepted Manuscript

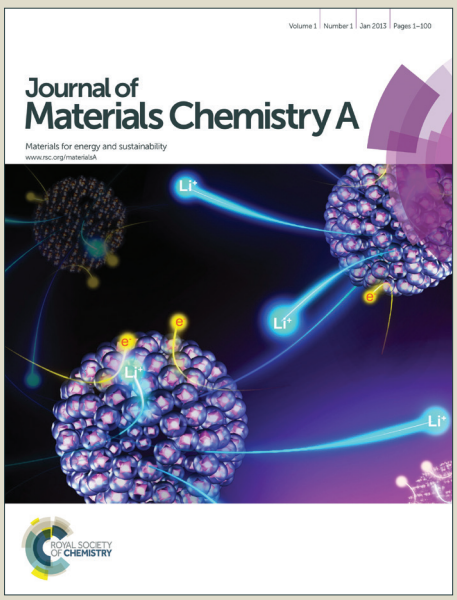

ROYAL SOCIETY OF CHEMISTRY

www.rsc.org/materialsA

Cite this: DOI: 10.1039/c0xx00000x

www.rsc.org/xxxxxx

ARTICLE TYPE

Graphene-Bacteria Composite for Oxygen Reduction and Lithium Ion Battery

Xuewan Wang,[a] Wei Ai,[b] Nan Li,[a] Ting Yu[b] and Peng Chen*[a]

Received (in XXX, XXX) Xth XXXXXXXXX 20XX, Accepted Xth XXXXXXXXX 20XX

DOI: 10.1039/b000000x

Owing to its extraordinary properties, graphene materials have changed the landscapes of many areas. However, their applications (e.g., in energy conversion and storage) are often limited by the lack of intrinsic electrochemical activities and restacking between graphene sheets. In this work, we demonstrate the synthesis of heteroatom-doped graphene/bacteria composite using chemically-exfoliated graphene oxide as the precursor and *E.coli* as the reducing agent, spacer and doping source. As the proof-of-concept demonstrations, we show that the carbonaceous rGO/*E.coli* composite are excellent electrode material for oxygen reduction reaction and lithium ion battery.

1 Introduction

Owing to its large surface area, good conductivity and wide electrochemical potential window, graphene materials have been widely used for energy applications, [1-3] such as, oxygen reduction [4, 5] and lithium ion battery. [6, 7] However, pristine graphene is not electrochemically active and lacks of intrinsic catalytic abilities. Therefore in energy devices, electrochemically active nanomaterials (e.g., nanostructured metal oxides) are needed to be composited with graphene. [8-12] This complicates the synthesis process and those functional nanomaterials are not as chemically stable as graphene. Alternatively, heteroatom doping can endow graphene with good catalytic and electrochemical properties. [13-15] Nevertheless, it is often challenging to dope graphene, particularly, to co-dope multiple species of heteroatoms.

Graphene materials used in energy devices are usually prepared by chemical processes, involving oxidative chemical exfoliation from graphite and subsequent chemical reduction to restore damaged graphene lattices (thus impaired conductivity) to certain extent. Reduced graphene oxide (rGO) sheets obtained from these processes are still largely defective. In addition, the reduction processes typically involve and / or produce environmental hazards, e.g., the commonly used reducing agent hydrazine. Furthermore, restacking of rGO sheets is inevitable during chemical reduction. Mild, green, and restacking-free reduction methods are hence highly desired.

Here, bacteria (*E.coli*) are used as effective and environmental-friendly bio-agent to reduce GO sheets, and as spacers to prevent restacking of rGO sheets. As all the other living species on earth, bacteria are carbon-based life-forms with abundant heteroatoms (especially, N, P, and S). Therefore, they may serve as good precursors and doping agents to produce doped carbon materials. We show that thermal annealing of graphene-bacteria composite self-assembled from the reduction process yields a porous carbon composite with abundant heteroatom species naturally inherited from the bacteria. We further demonstrate the use of such novel graphene-bacteria composite as electrode material for high performance oxygen reduction (ORR) and lithium ion battery (LIB) applications.

2 Experimental sections

2.1 Preparation of carbonaceous rGO/*E.coli* composite

GO was prepared from graphite powder using a modified Hummers method. [16] *E.coil* bacteria were firstly inoculated into 20 mL fresh Luria broth (LB; 10 g L^{-1} tryptone, 5 g L^{-1} yeast extract, 10 g L^{-1} NaCl, pH 7.0) and incubated overnight at 37 °C with shaking rate of 200 rpm. 30 mg GO was added into 150 mL fresh LB followed by 10 min ultra-sonication (LB-GO). The cultured bacteria were harvested and re-suspended in LB-GO broth with final optical density (OD_{600}) value of 0.3, followed by further incubation at 37 °C under aerobic condition and shaking rate of 200 rpm for 108 h. The resulting rGO-*E.coli* composite was collected, washed and lyophilized. Subsequently, the sample was annealed in a tube furnace in which the temperature gradually increases at 1°C min^{-1} and maintains at to 900 °C for 2 h. The resulting composite was washed overnight by 3 M HCl at 100 °C to remove the salts and impurities, and finally lyophilized for use.

2.2 Materials characterization

The samples were examined with scanning electron microscopy (JSM-6700F, JEOL), Raman spectroscopy (Renishaw InVia

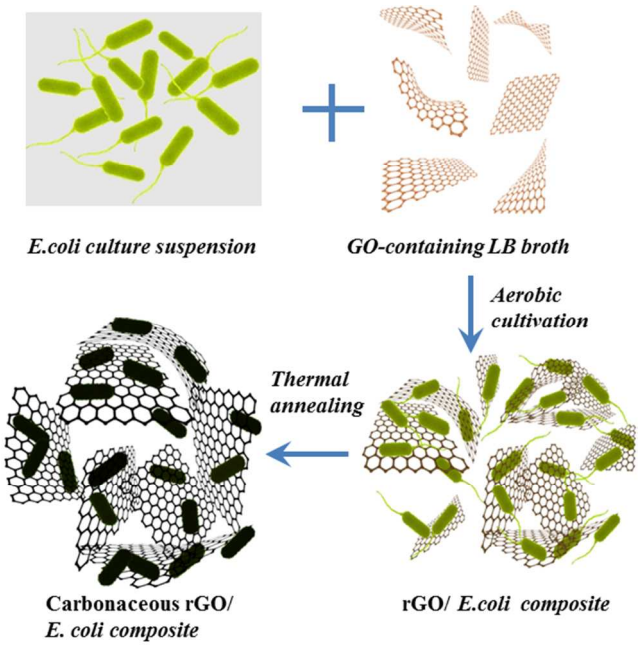

Fig. 1 Schematic illustration of synthesis of carbonaceous rGO/*E.coli* composite.

Reflex Raman system with laser excitation wavelength of 514 nm), X-ray diffraction spectroscopy (Bruker D8 Advance Diffractometer using Cu Ka radiation), Fourier transform infrared spectroscopy (PerkinElmer Spectrum GX FTIR system), SEM element mapping (JSM-7100F, JEOL), X-ray photoelectron spectroscopy (Kratos Axis Ultra^{DLD} spectrometer with a monochromatized Al Kα X-ray source), Nitrogen adsorption-desorption isotherm (Quantachrome AUTOSORB-1), and transmission electron microscopy (TEM, JEM-3010, with an accelerating voltage of 200 kV, JEOL).

2.3 Electrochemical measurements for ORR

Electrochemical measurements were performed on a CHI-760D electrochemical workstation using a three-electrode configuration with a Pt wire as the counter electrode and an Ag/AgCl electrode as the reference. Cyclic voltammetry (CV) was conducted in KOH (0.1 M) electrolyte in the potential window from -1.0 to 0.2 V at the sweep rate of 10 mV s^{-1}. Using rotating disk electrode, the polarization curves were obtained at scan rate of 5 mV s^{-1}, rotating speed varying from 400 to 2025 rpm, and holding potential from 0.2 to -0.8 V. Before the each measurement, the electrolyte was bubbled with O_2 over 20 min. To prepare the working electrode, 5 mg of carbonized rGO/E.coli sample was dispersed into a solution containing 0.9 mL of deionized water and 0.1 mL of 5 wt% Nafion aqueous solution, and ultrasonicated to form a homogenous solution. Subsequently 20 uL of the obtained solution was deposited onto a glassy carbon electrode (GC, 5 mm in diameter) and dried at 50 ˚C. GC electrode coated with commercial Pt/C (20 wt%, Premetek) was measured for comparison. The loading amount of Pt/C is optimized to give the best performance.

2.4 Electrochemical measurements for LIB

The electrochemical performance of carbonized rGO/E.coli composite for Li storage was evaluated in 2032 coin-type cells

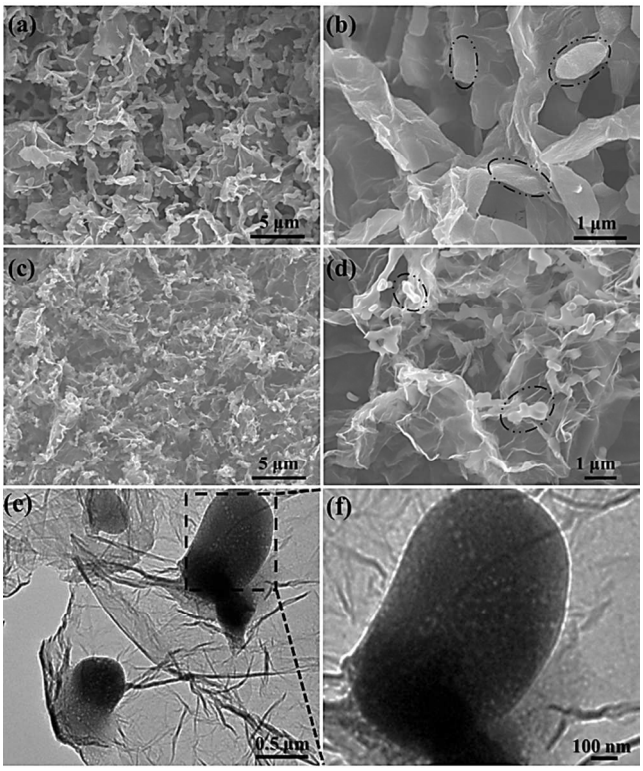

Fig. 2 SEM images of rGO/*E.coli* (a, b) before and (c, d) after thermal annealing. The dashed ovals in (b) and (d) highlight the bacterial cells. (e) TEM images of rGO/*E.coli* after thermal annealing. (f) Zoom-in view of a carbonized bacteria in (e).

assembled in argon-filled glove box. To make the LIB anode, carbonaceous rGO/*E.coli* sample, acetylene black, and poly(vinylidene fluoride) with mass ratio of 80:10:10 were mixed with N-methyl-2-pyrrolidone to form a homogeneous slurry, which was then coated onto a copper foil current collector and dried at 100 °C overnight under vacuum. Pure lithium metal served as both counter electrode and reference electrode. 1 M $LiPF_6$ solution in a mixture of ethylene carbonate and dimethyl carbonate (1:1, v/v) serves as the electrolyte. The cells were galvanostatically charged and discharged using a Neware battery testing system in the voltage range of 0.005 – 3.0 V (*vs.* Li/Li^+). Cyclic voltammetry (CV) was carried on a CHI-760D electrochemical workstation over potential window of 0.005 to 3 V at the scan rate of 0.5 mV s^{-1}.

3 Results and discussion

The synthetic procedure of carbonaceous graphene-bacteria composite is illustrated in Fig. 1. It has been reported that GO sheets with rich oxygenated groups can act as terminal electron acceptors for the bacterial respiration process, leading to their reduction. [17, 18] In agreement with this notion, we observe that yellowish GO dispersion gradually becomes dark after addition of *E.coli* bacteria (Fig. S1 in Electronic Supplementary Information). The rGO/*E.coli* hybrids collected by centrifugation are subsequently lyophilized and subjected to thermal annealing at 900 °C to carbonize *E.coli* and further reduce rGO sheets.

As revealed by scanning electron microscopy (SEM), the lyophilized rGO/*E.coli* composite is a porous network with

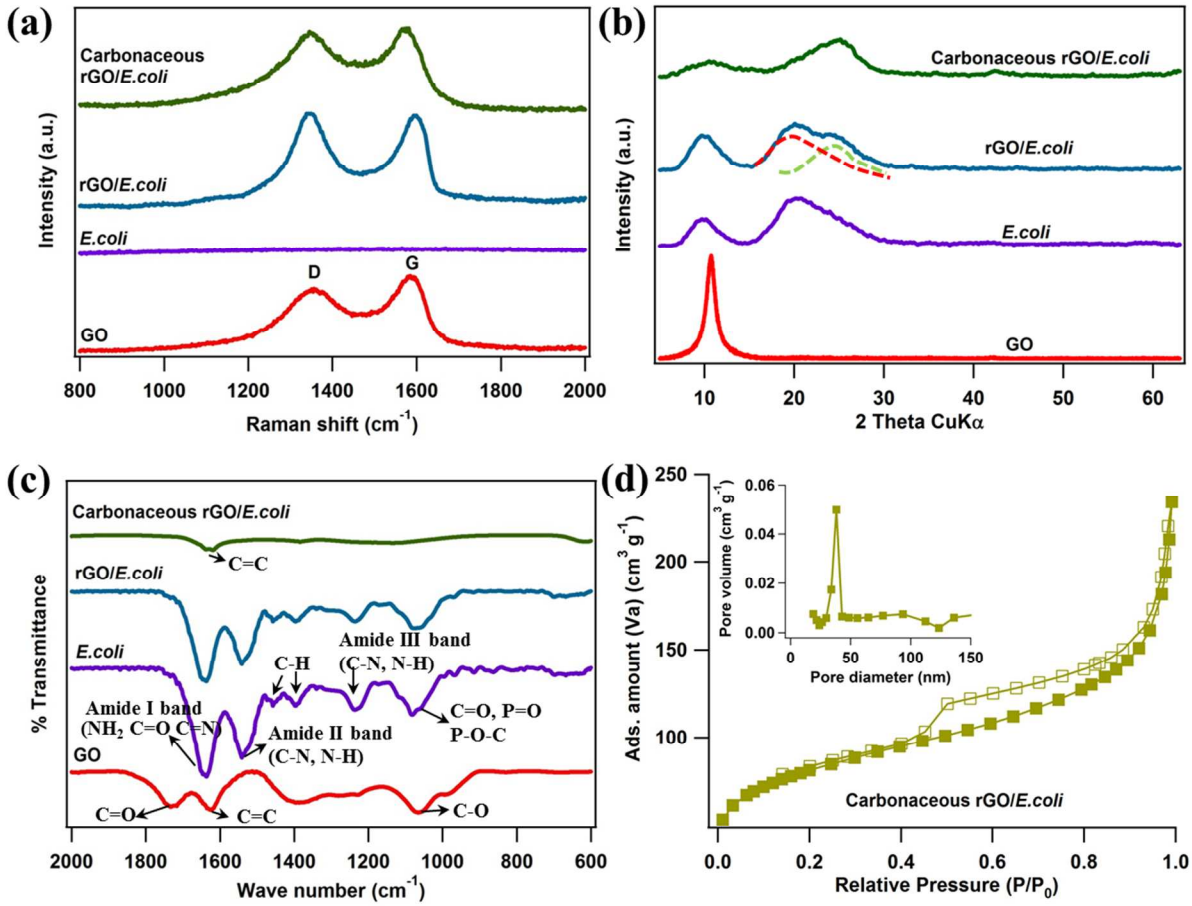

Fig. 3 (a) Raman spectra, (b) XRD patterns, (c) FTIR spectra, (d) nitrogen adsorption and desorption isotherm of the prepared samples. Inset in (d) shows the pore size distribution of carbonaceous rGO/*E.coli* composite.

numerous *E.coil* cells (~1 μm) attached onto or encapsulated by rGO microsheets (Fig. 2a and b). The mild and gradual reduction process allows uniform mixture of *E.coli* and rGO without severe aggregation of bacteria or rGO sheets. In addition, bacteria serve as spacers to prevent stacking between hydrophobic rGO sheets. After thermal annealing, the resulting carbonaceous rGO/*E.coli* composite retains the microporous structure except that the carbonized bacteria largely shrink in size (Fig. 2c and d). As revealed by TEM (Fig. 2e and f), mesopores (< 50 nm) appear on the surface of carbonized bacteria. Thermal annealing also further reduces rGO, enhances coupling between rGO and *E.coli*, and possibly induces heteroatom-doping on rGO due to generation of reactive species from decomposition of bacterial components.

Raman spectroscopy shows that rGO/*E.coli* exhibits an increased D/G intensity ratio as compared with GO (Fig. 3a). This is attributed to the restoration of graphitic C=C bonds and consequent increase in the number of small sp^2 domains. [19] Both D and G bands of the carbonaceous rGO/*E.coli* is widened because of low-crystalline structures from carbonized bacteria and possibly disorders induced by heteroatom doping. X-ray diffraction (XRD) pattern of GO shows a characteristic (002) diffraction peak at 10.74° indicating interlayer spacing of ~8.24 Å (Fig. 3b). In addition to the two broad peaks from *E.coli*, the XRD pattern of rGO/*E.coli* also shows a shifted and widened (002) diffraction peak at 24° corresponding to interlayer spacing of ~3.71 Å. This confirms the bio-reduction (thus removal of oxygenated functional groups) of GO sheets. After thermal annealing, the XRD pattern of carbonaceous rGO/*E.coli* exhibits a broadened characteristic rGO peak at ~25° with much reduced components inherited from *E.coli*. The Fourier transform infrared spectroscopy (FTIR) spectrum of rGO/*E.coli* exhibits characteristic peaks of various functional groups (e.g. NH_2, C=N, CH_2/CH_3, P=O, C-O-P, C=O, C-O-C, C=C) from biomolecules in *E.coli* (Fig. 3c). [20] And as compared to GO, the C=O peak at 1730 cm^{-1} vanishes due to removal of COOH groups from GO sheets after effective bio-reduction. [21] In contrast, FITR spectrum of carbonized rGO/*E.coli* presents a dominating graphitic C=C peak at 1626 cm^{-1}, indicating essential removal of chemical groups. Based on N_2 adsorption/desorption measurement using Brunauer-Emmett-Teller (BET) model (Fig. 3d), the porous structure of carbonized rGO/*E.coli* gives a specific surface area of 288 m^2 g^{-1}, which is larger than that of rGO aerogel obtained by lyophilisation of pure rGO sheets, [22] P-doped graphene [23] and N-, S-codoped graphene obtained by thermal annealing of 2-aminothiophenol functionalized GO. [24] Also as shown in Fig. 3d and the (inset), the composite is a mesoporous material with a narrow mesopore size distribution.

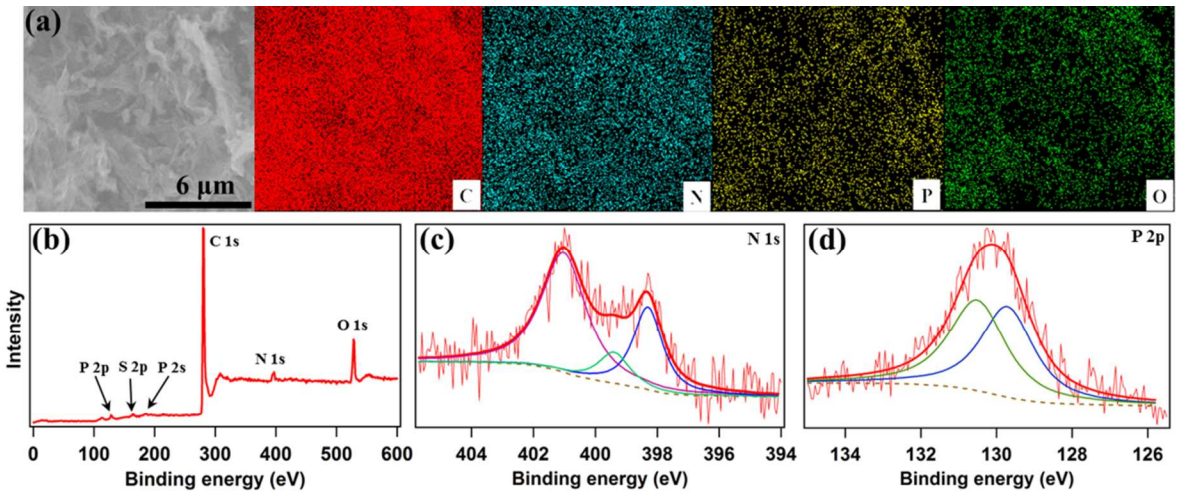

Fig. 4 (a) SEM-EDS mapping, and (b-d) XPS analyses of carbonaceous rGO/*E.coli* composite.

SEM-energy dispersive spectroscopic (SEM-EDS) mapping for carbonaceous rGO/ E.coli shows abundant and uniform distribution of C, N, O, and P (Fig. 4a). The observation suggests that these heteroatoms are not only confined in carbonized bacteria but also uniformly doped onto rGO sheets. Consistently, X-ray photoelectron spectroscopy (XPS) spectrum demonstrates the characteristic peaks of P2p at 130 eV, S2p at 164 eV, C1s at 284 eV, N1s at 400 eV and O1s at 532 eV (Fig. 4b). [25, 26] The atomic concentrations of N, P and S are 2.42%, 1.25% and 0.42% respectively. The high resolution N1s spectrum can be deconvoluted into three peaks corresponding to pyridinic- (28 at%), pyrrolic- (11 at%) and graphitic- (61 at%) N species (Fig. 4c). The high resolution P2p peak can be resolved into two peaks corresponding to P-C (48.2 at%) and P-O (51.8 at%) (Fig. 4d). [27]

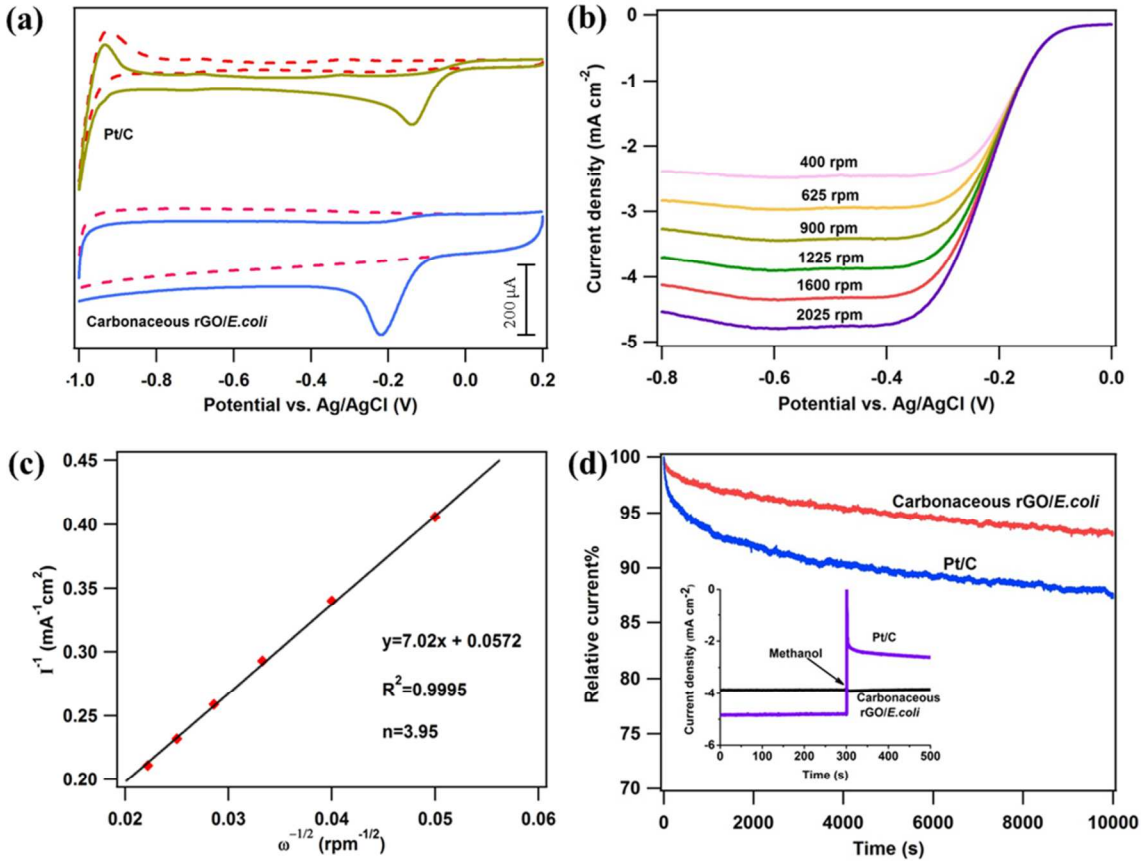

Fig. 5 (a) CV curves of carbonaceous rGO/*E.coli* and Pt/C in O_2-saturated (solid line) and N_2-saturated (dashed line) 0.1 M KOH solutions with a scan rate of 10 mV s^{-1}. (b) RDE (rotating disk electrode) voltammograms of carbonaceous rGO/E.coli in O_2-saturated 0.1 M KOH at a scan rate of 5 mV s^{-1} and various rotation speeds. (c) Koutecky-Levich (K-L) plot at -0.4 V vs. Ag/AgCl. (d) Normalized chronoamperometric curves of carbonaceous rGO/E.coli and commercial Pt/C at -0.4 V vs. Ag/AgCl in O_2-saturated 0.1 M KOH solution. Inset shows the interference by addition of 2% v/v methanol.

Heteroatom doping endows graphene with catalytic properties. Both N-doped and P-doped graphene have been used for oxygen reduction reaction (ORR) which is the rate-limiting cathodic reaction in energy devices (e.g., fuel cells, Li-air batteries). [28, 29] As shown in Fig. 5a, cyclic voltammetry (CV) of carbonaceous rGO/*E.coli* exhibits a prominent reduction peak in the presence of oxygen, demonstrating its catalytic activity towards ORR. Fig. 5b depicts linear-sweep voltammetry curves at different rotation speeds. The onset potential is ~-0.09V which is not far from that of Pt/C electrode (0 V) and superior to previously reported doped graphene materials. [30-32] Also as shown, the current density reaches steady-state at the overpotential as low as ~0.38 V even at the high rotation speed of 1600 rpm, implying the high efficiency of ORR. The slight decrease of current density at high overpotentials (>0.6 V) is because replenishment of oxygen by diffusion lags behind the rapid reduction reaction. [33]

The electron transfer kinetics is analysed by the Koutecky-Levich (K-L) plot at the potential of -0.4 V (Fig. 5c). The good linear fitting signifies a first order reaction and its slope indicates an electron-transfer number of 3.95 (derivation in ESI). Such efficient four-electron process preserves even at a high overpotential (0.8 V). As shown in Fig. S3 (ESI), rGO/*E.coli* and Pt/C exhibit comparable Tafel slopes at low currents, indicating that the rate-limiting step for both materials at low currents is the first electron transfer step and confirming the similar electrocatalytic activity of both materials.[34] The excellent electrocatalytic property of carbonaceous rGO/*E.coli* composite is attributable to the enriched and well-exposed active sites and the synergistic effects of multi-dopants. Co-existence of multiple species of heteroatoms can introduce asymmetric spins and charge polarization in graphene lattice whereby improve electrocatalytic activity. [13, 35, 36] For example, it has been reported that introducing S and O atoms into N-doped nanoporous carbon further enhances its electrocatalytic activity towards ORR. [37] The performance of rGO/*E.coli* is superior to the previously reported ternary (N, P, B)-doped porous nanocarbons, [38] N and S co-doped graphene, [24] N doped graphene, [30] and sulfonic acid-functionalized graphene nanoplates. [39]

Although the onset potential of carbonaceous rGO/E.coli is not as ideal as Pt/C (Fig. S2 in ESI), it exhibits better durability because of its higher resistance to electrochemical oxidation (Fig. 5d). Methanol is a readily available and widely used fuel for fuel cells. However, the commercialization of direct methanol fuel cells is seriously hindered by the toxification of platinum by methanol crossover from anode to cathode through the membrane. In contrast, our rGO/E.coli shows remarkable tolerance to methanol (Fig. 5d, inset).

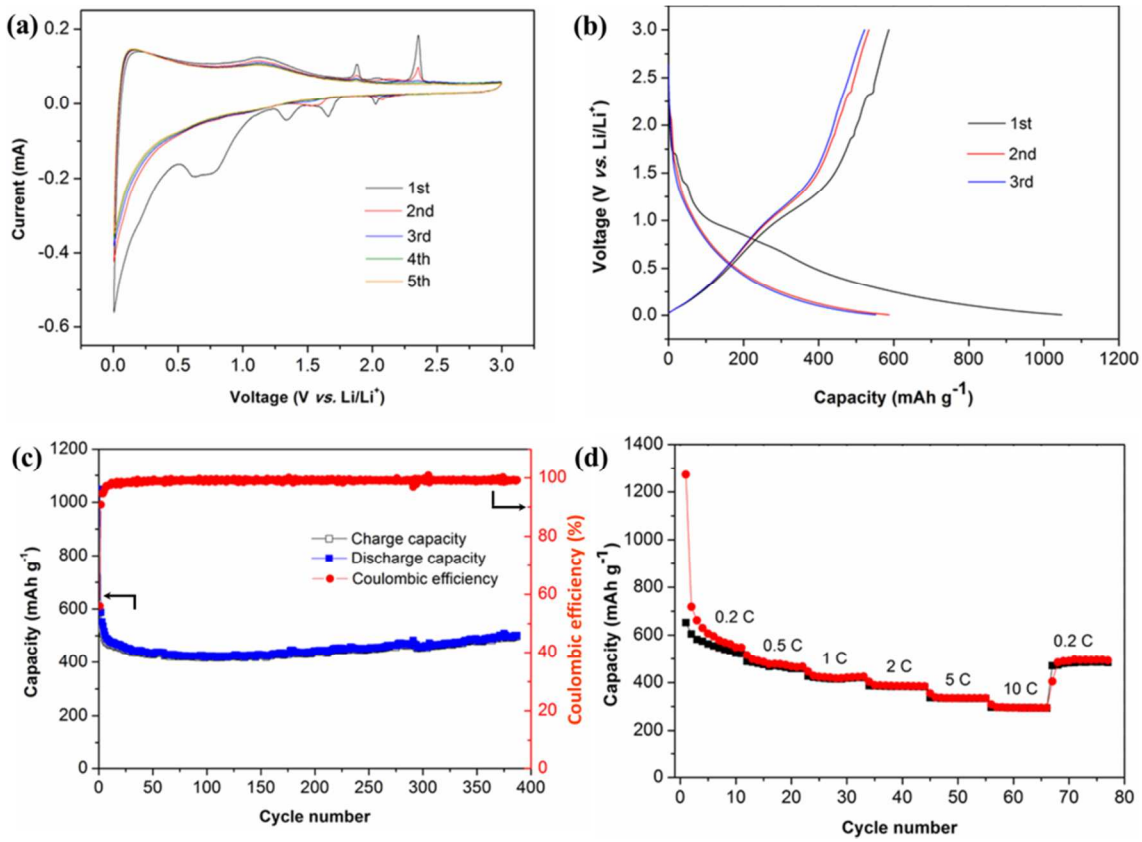

Fig. 6 (a) CV curves of carbonaceous rGO/*E.coli* at a scan rate of 0.5 mV s^{-1}. (b) Galvanostatic charge-discharge profiles at current density of 0.5 C. (c) Cycling performance and Coulombic efficiency of rGO/*E.coli* electrode at 0.5 C between 0.005 and 3 V *vs.* Li^+/Li. (d) Rate performance of rGO/*E.coli* electrode charged between 0.005 and 3V vs. Li^+/Li at various current densities.

Heteroatom-doped graphene nanomaterials have also been considered as promising electrode materials for lithium ion battery (LIB). [40] Fig. 6a depicts the first five CVs of carbonized rGO/E.coli as the anode material for LIB. The strong reduction peak at 0.5~1.0 V in the first cycle is the indicator of the formation of solid-electrolyte interphase (SEI) film on the electrode surface. [27] Notably, there are a few small redox peaks (specifically, oxidation peaks at ca. 1.2, 1.8 and 2.4 V, reduction peaks at ca. 1.3, 1.7 and 2.1 V) in the first two cycles, which are likely resulted from the irreversible binding and delithiation of Li ions caused by defects, dopants and oxygen-containing functional groups on the carbonaceous rGO/*E.coli* composite. [13] From the third cycle onwards, the CV curves overlap demonstrating the good stability and reversibility of the electrode.

As shown in Fig. 6b, carbonaceous rGO/*E.coli* shows an initial discharge capacity of 1048 mAh g^{-1} and reversible capacity of 587 mAh g^{-1} at current density of 0.5 C (1 C means the theoretical capacity of graphite, 372 mAh g^{-1}, can be charged or discharged within 1 h). The plateau in the discharge profile at ~0.9 V can be ascribed to the formation of SEI film on the electrode surface. The irreversible capacity loss in the first cycle is ascribed to the consumption of Li by defects and dopants, the initial formation of SEI, as well as electrolyte decomposition. After the initial decrease, the discharging capacity of rGO/*E.coli* electrode gradually increases reaching a value of 501.5 mAh g^{-1} at the 380th cycle (Fig. 6c). The increase of discharging capacity may be attributed to the electrochemical activation of electrode materials and/or enhanced accessibility of Li ions during cycling. This observation indicates the remarkable cycling stability of the electrode. And the Coulombic efficiency retains at 97~ 99% from the 5th cycle onwards. Fig. 6d presents the rate performance of rGO/E.coli electrode at 0.2 to 0.5, 1, 2, 5, 10 C. This heteroatom-doped electrode outperforms the previously reported undoped 3D graphene (308 mAh g^{-1} at 50 mA g^{-1}), [41] N-doped graphene (~ 200 mAh g^{-1} at 2 C), [42] P-doped graphene (~ 200 mAh g^{-1} at 2 A g^{-1}), [27] and phenolic resin-grafted rGO (212.3 mA h g^{-1} at 2 A g^{-1}). [43] In addition, the capacity can be completely restored once the current rate returns to the initial 0.2 C. Taken together, our electrode demonstrates excellent rate performance and reversibility.

4 Conclusions

In summary, a hybrid graphene structure doped with multiple heteroatom species has been fabricated by a facile and green method using bacteria as the reducing agent, spacer, and doping source. Such rGO/*E.coli* composite promises a wide range of applications, including electrocatalysis, sensing, energy storage and conversion. As the proof-of-concept demonstrations, we show its superior performance in oxygen reduction reaction and lithium ion battery. This is attributable to the excellent catalytic and electrochemical activities endowed by the synergistic effects of co-dopants. In addition, the porous structure of the composite offers large surface area, good ion accessibility, and abundant active edge sites.

Acknowledgements

This work was supported by the Singapore Ministry of Education under the AcRF Tier 2 grants (MOE2011-T2–2–010, MOE2014-T2-1-003).

Notes and references

[a] *School of Chemical and Biomedical Engineering, Nanyang Technological University, 70 Nanyang Drive, 637457, Singapore. Fax: 65 6791 1761; Tel: 65 6514 1086; E-mail: ChenPeng@ntu.edu.sg*
[b] *School of Physical and Mathematical Sciences, Nanyang Technological University, 21 Nanyang Link, 637371, Singapore*

† Electronic Supplementary Information (ESI) available. See DOI: 10.1039/b000000x/

1. J. Liu, *Nat Nanotechnol*, 2014, **9**, 739-741.
2. F. Bonaccorso, L. Colombo, G. H. Yu, M. Stoller, V. Tozzini, A. C. Ferrari, R. S. Ruoff and V. Pellegrini, *Science*, 2015, **347**, 6217.
3. S. Han, D. Q. Wu, S. Li, F. Zhang and X. L. Feng, *Adv Mater*, 2014, **26**, 849-864.
4. S. J. Guo and S. H. Sun, *J Am Chem Soc*, 2012, **134**, 2492-2495.
5. X. J. Zhou, J. L. Qiao, L. Yang and J. J. Zhang, *Adv Energy Mater*, 2014, **4**, 130523.
6. X. S. Zhou, L. J. Wan and Y. G. Guo, *Adv Mater*, 2013, **25**, 2152-2157.
7. W. W. Sun and Y. Wang, *Nanoscale*, 2014, **6**, 11528-11552.
8. S. Bag, K. Roy, C. S. Gopinath and C. R. Raj, *Acs Appl Mater Inter*, 2014, **6**, 2692-2699.
9. J. W. Lee, S. Y. Lim, H. M. Jeong, T. H. Hwang, J. K. Kang and J. W. Choi, *Energ Environ Sci*, 2012, **5**, 9889-9894.
10. S. Mayavan, H. S. Jang, M. J. Lee, S. H. Choi and S. M. Choi, *J Mater Chem A*, 2013, **1**, 3489-3494.
11. D. P. Dubal, R. Holze and P. Gomez-Romero, *Sci Rep-Uk*, 2014, **4**, 7349.
12. S. Chen and S. Z. Qiao, *Acs Nano*, 2013, **7**, 10190-10196.
13. X. W. Wang, G. Z. Sun, P. Routh, D. H. Kim, W. Huang and P. Chen, *Chem Soc Rev*, 2014, **43**, 7067-7098.
14. X. K. Kong, C. L. Chen and Q. W. Chen, *Chem Soc Rev*, 2014, **43**, 2841-2857.
15. A. Dhakshinamoorthy, A. Primo, P. Concepcion, M. Alvaro and H. Garcia, *Chem-Eur J*, 2013, **19**, 7547-7554.
16. S. L. Ting, C. X. Guo, K. C. Leong, D. H. Kim, C. M. Li and P. Chen, *Electrochim Acta*, 2013, **111**, 441-446.
17. S. Gurunathan, J. W. Han, V. Eppakayala and J. H. Kim, *Colloid Surface B*, 2013, **102**, 772-777.
18. G. M. Wang, F. Qian, C. Saltikov, Y. Q. Jiao and Y. Li, *Nano Res*, 2011, **4**, 563-570.
19. H. B. Feng, R. Cheng, X. Zhao, X. F. Duan and J. H. Li, *Nat Commun*, 2013, **4**, 1539.
20. Z. Filip, S. Hermann and K. Demnerova, *Czech J Food Sci*, 2008, **26**, 458-463.
21. Z. Z. Du, W. Li, W. Ai, Q. Tai, L. H. Xie, Y. Cao, J. Q. Liu, M. D. Yi, H. F. Ling, Z. H. Li and W. Huang, *Rsc Adv*, 2013, **3**, 25788-25791.
22. W. F. Chen, S. R. Li, C. H. Chen and L. F. Yan, *Adv Mater*, 2011, **23**, 5679-5683.
23. Y. Y. Wen, B. Wang, C. C. Huang, L. Z. Wang and D. Hulicova-Jurcakova, *Chem-Eur J*, 2015, **21**, 80-85.
24. W. Ai, Z. M. Luo, J. Jiang, J. H. Zhu, Z. Z. Du, Z. X. Fan, L. H. Xie, H. Zhang, W. Huang and T. Yu, *Adv Mater*, 2014, **26**, 6186-6192.
25. A. G. Kannan, J. Zhao, S. G. Jo, Y. S. Kang and D. W. Kim, *J Mater Chem A*, 2014, **2**, 12232-12239.
26. J. S. Li, S. L. Li, Y. J. Tang, K. Li, L. Zhou, N. Kong, Y. Q. Lan, J. C. Bao and Z. H. Dai, *Sci Rep-Uk*, 2014, **4**, 5130.
27. C. Z. Zhang, N. Mahmood, H. Yin, F. Liu and Y. L. Hou, *Adv Mater*, 2013, **25**, 4932-4937.
28. R. Li, Z. D. Wei, X. L. Gou and W. Xu, *Rsc Adv*, 2013, **3**, 9978-9984.
29. M. Borghei, I. Azcune, P. M. Carrasco, J. Sainio, E. Kauppinen and V. Ruiz, *Int J Hydrogen Energ*, 2014, **39**, 12749-12756.
30. Y. W. Zhang, J. Ge, L. Wang, D. H. Wang, F. Ding, X. M. Tao and W. Chen, *Sci Rep-Uk*, 2013, **3**, 2771.
31. F. X. Ma, J. Wang, F. B. Wang and X. H. Xia, *Chem Commun*, 2015, **51**, 1198-1201.
32. Y. Z. Su, Y. Zhang, X. D. Zhuang, S. Li, D. Q. Wu, F. Zhang and X. L. Feng, *Carbon*, 2013, **62**, 296-301.
33. J. Liang, Y. Zheng, J. Chen, J. Liu, D. Hulicova-Jurcakova, M. Jaroniec and S. Z. Qiao, *Angew Chem Int Edit*, 2012, **51**, 3892-3896.
34. C. J. Song and J. J. Zhang, *PEM Fuel Cell Electrocatalysts and Catalyst Layers*; J. J. Zhang, Ed.; Springer: London, 2008; pp 89-134.
35. I. Y. Jeon, H. J. Choi, M. Choi, J. M. Seo, S. M. Jung, M. J. Kim, S. Zhang, L. P. Zhang, Z. H. Xia, L. M. Dai, N. Park and J. B. Baek, *Sci Rep-Uk*, 2013, **3**, 1810.
36. I. Y. Jeon, S. Zhang, L. P. Zhang, H. J. Choi, J. M. Seo, Z. H. Xia, L. M. Dai and J. B. Baek, *Adv Mater*, 2013, **25**, 6138-6145.
37. Y. Y. Meng, D. Voiry, A. Goswami, X. X. Zou, X. X. Huang, M. Chhowalla, Z. W. Liu and T. Asefa, *J Am Chem Soc*, 2014, **136**, 13554-13557.
38. S. Y. Zhao, J. Liu, C. X. Li, W. B. Ji, M. M. Yang, H. Huang, Y. Liu and Z. H. Kang, *Acs Appl Mater Inter*, 2014, **6**, 22297-22304.
39. I. Y. Jeon, H. J. Choi, S. M. Jung, J. M. Seo, M. J. Kim, L. M. Dai and J. B. Baek, *J Am Chem Soc*, 2013, **135**, 1386-1393.
40. B. Quan, S. H. Yu, D. Y. Chung, A. H. Jin, J. H. Park, Y. E. Sung and Y. Z. Piao, *Sci Rep-Uk*, 2014, **4**, 5639.
41. C. X. Guo, M. Wang, T. Chen, X. W. Lou and C. M. Li, *Adv Energy Mater*, 2011, **1**, 736-741.
42. M. Du, J. Sun, J. Chang, F. Yang, L. J. Shi and L. Gao, *Rsc Adv*, 2014, **4**, 42412-42417.
43. M. C. Li, H. H. Song, X. H. Chen, J. S. Zhou and Z. K. Ma, *Phys Chem Chem Phys*, 2015, **17**, 3250-3260.

Text: Heteroatom-doped graphene/bacteria composite exhibits superior performance for oxygen reduction and lithium ion storage.

Colour graphic: